This document is the Accepted Manuscript version of the following article: Xiangkui Aao, Yanping Yuan, Hongwei Wu, and Xudong Zhao, 'Coupled Cooling Method and Application of Latent Heat Thermal Energy Storage Combined with Pre-cooling of Envelope: Sensitivity Analysis and Optimization', *Process Safety and Environmental Protection,* first published online 9 March 2017.

The version of record is available online at doi: http://dx.doi.org/10.1016/j.psep.2017.03.005

Coupled Cooling Method and Application of Latent Heat Thermal Energy Storage Combined with Pre-cooling of Envelope: Sensitivity Analysis and Optimization

Gao Xiangkui[1] *Yuan Yanping**[1] *Cao Xiaoling*[1] *Wu Hongwei*[2] *Zhao Xudong*[3]

[1]School of Mechanical Engineering, Southwest Jiaotong University, 610031 Chengdu, China

[2]School of Engineering and Technology, University of Hertfordshire, Hatfield, AL10 9AB, United Kingdom

[3]School of Engineering, Faculty of Science, University of Hull, Hull, HU6 7RX, United Kingdom

Abstract: Cooling system for mine refuge chamber provides comfortable environment for miners to avoid heat damage. The existing cooling systems have their own application scopes and limitations. The coupled cooling method of Latent Heat Thermal Energy Storage (LHTES) combined with Pre-cooling of Envelope (PE) is a new free cooling method which is suitable for high-temperature, passive, impact and other harsh environment. Then, to improve the thermal comfort and reduce energy consumption, the effect of the pre-cooling temperature, melting temperature of PCM, aspect ratio and amounts of PCM unit on the indoor temperature are investigated in a systematic manner. Furthermore, the system is optimized and the generalized results for the evaluation parameter are given. Analysis of the results may lead to following main conclusions: (i) the method really controls the indoor temperature and the saving amount of PCM is more than 50% compared to the traditional LHTES systems; (ii) the Temperature Control(TC) performance of PCM would drop significantly if it melts more than 80%; (iii) under current operating conditions, the optimal melting temperature is about 29℃ and the aspect ratio of PCM unit is 60:500; (iv) per 1℃ the pre-cooling temperature dropped, 19% the actual amount of PCM decreased for the case studied.

Keywords: Coal mine accident; Refuge chamber; Cooling method; Latent Heat Thermal Energy Storage; Surrounding rock; Thermal analysis.

Nomenclature

a	thermal diffusivity, m^2/s
A	area, m^2
c_P	specific heat, J/(kg·K)

30	g	acceleration of gravity,m/s^2
31	h	convective heat transfer coefficient, W/(m^2·K)
32	H	high, m
33	l	feature size, m
34	L	length, m
35	N	number
36	q	heat flux, W
37	Q	heat, J
38	r	radius, m
39	t	temperature,℃
40	V	voltage, m^3
41	W	width, m
42	**Greek symbols**	
43	α	expansion coefficient
44	γ	the evaluation parameter of heat tolerance time
45	δ	thickness, m
46	Δ	difference
47	λ	thermal conductivity, W/(m·K)
48	ρ	density, kg/m^3
49	τ	time, s
50	υ	viscosity, m^2/s
51	**Subscripts**	
52	a	air
53	e	extreme endurance
54	f	flow air
55	i	inner/indoor
56	m	melt
57	o	outer
58	pc	pre-cooling
59	P	person
60	R	refuge chamber
61	$R1$	side wall of refuge chamber
62	$R2$	vault of refuge chamber
63	w	wall
64	0	initial value
65	**Abbreviation**	
66	ETCP	Effective Temperature Control Period
67	LHTES	Latent Heat Thermal Energy Storage
68	PE	Pre-cooling of Envelope
69	PCM	Phase Change Material
70	SR	Surrounding Rock
71	TC	Temperature Control
72	UDF	User Define Function
73	**Dimensionless numbers**	

74 *Gr* Grashof number
75 *Nu* Nusselt number
76 *Pr* Prandtl number

77 1. Introduction

78 In Aircraft, defense engineering, mine refuge and some other facilities [1-2], there still exists
79 some special spaces with high-temperature and no-power in certain circumstances. Taking the
80 underground mine refuge chamber [1] as an example, it's an important emergency rescue shelter,
81 which provides sufficient time for the trapped miners to wait for the rescue. When the mine
82 accident happens, the refuge chamber will become an isolated, hot and humid space, depending on
83 the internal as well as the environmental condition and there is no power supply. As shown in
84 Table 1, the existing cooling methods, which consist of CO_2 phase change cooling, the explosion
85 proof electrical air conditioning, the ventilation cooling and the ice storage cooling, have their
86 own application scopes and limitations [3]. LHTES system also cannot control the temperature
87 independently due to the large cold loads [4] or the small operating temperature range.

88 Table 1. Evaluation and application of four cooling methods.

cooling methods	advantages	disadvantages	application
CO_2 phase change cooling	No need of electric power; Stability	The risk of leakage; Regular inspection and replacement are needed; The difficulty to maintain	Where the ambient temperature is below 31℃
Explosion proof air conditioning	Excellent cooling effect; Convenient adjustment	The refrigerator may not work when the gas explosion occurs; Intrinsically safe high power battery is needed	Metallic/ nonmetallic Mine
Ventilation cooling	No safety hazard; With air purification function	Ventilation ducts may be damaged; Poor cooling effect in a deep buried depth	Shallow mine
Ice storage cooling	No safety hazard; Stability	Compressor is easily eroded; High maintenance cost; Taking up large valuable living space; The fan is needed	Any conditions

88

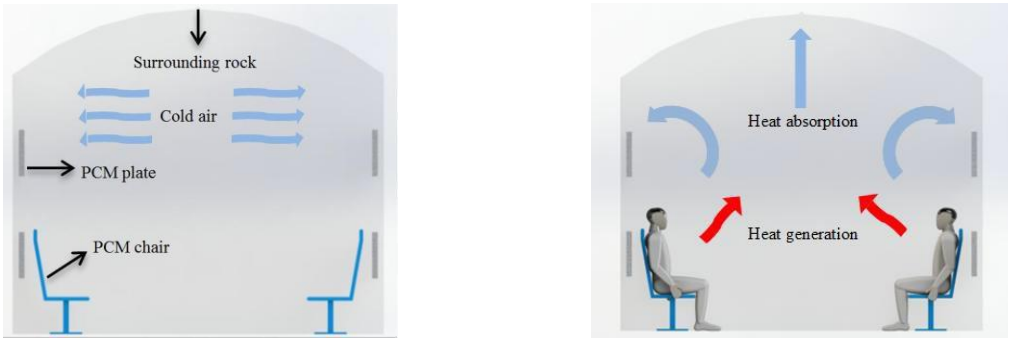

(a) (b)

Fig. 1. Schematic of the coupled cooling method of LHTES combined with PE: (a) PE in peacetime; (b) Heat storage of LHTES and envelope in working time.

To solve this problem, a new coupled cooling method of LHTES combined with pre-cooling of envelope is proposed by Yuan et al [5]. As shown in Fig. 1(a), the envelope is pre-cooled by forced-air in peacetime and the PCM of suitable temperature are encapsulated into units to store cold. As shown in Fig. 1(b), fully using sensible heat storage capacity of envelope and latent heat storage capacity of PCM can control the temperature in working time.

The coupled cooling method can not only expand the operating temperature difference of PCM, but also bear numerous cold loads to reduce the amount of PCM by pre-cooling the envelop. This method meets the requirements of safety, no power, stability and reliability under special environment and widens the application range of LHTES system for temperature control.

In order to save energy, the natural cold source, such as low-temperature water (the water temperature is less than 15℃), cold air (winter), snow or ice, should be fully utilized. When the natural cold source cannot meet the pre-cooling demand, the cold air from the mining working face should be partly shunted into the refuge chamber. And intermittent cold storage technology can be used since the thermal diffusivity of the rock is small and there is no heat source in the room. As a consequence, the indoor temperature could not have a remarkable rise during a rest period.

In theory, LHTES can not only reduce the mismatch between supply and demand but also improve the performance and reliability of energy systems [6]. In fact, many places of LHTES should be optimized and improved in the application process. Over the past decades, extensive research efforts have been made on the sensitivity analysis and optimization for different LHTESs [7-12].

Sensitivity analysis and optimization of the PCM unit can enhance the effectiveness of heat transfer. The operation characteristics and influencing factors of the PCM unit mainly involve the natural convection, the arrangement of fins and the change of unit structure. To improve the thermal storage performance of the circular finned tube, the influence factors such as the fin pitch, the fin height, the fin thickness and the inner radius of the tube, were numerically investigated by Wang et al [13]. A recent study of Yuan et al [14] mainly focused on the fin angle's influence on the heat storage rate of annular PCM unit. Their results showed that there existed maximum melting heating rate when the fins are vertical. Borderon et al [15] designed a new PCM-air heat transfer ventilation system based on the night ventilation unit. To ensure the air heat exchanger can adapt to different climatic conditions, running different ventilation conditions should correspond to the external environments to achieve the optimum utilization of cold. Solgi et al [16] also studied the PCM-air heat exchanger and tried to find the suitable condition to start the night ventilation. It was found that the composite PCM for heat storage will greatly reduce the indoor load.

The operation characteristics and influencing factors of the PCM envelope mainly focused on the selection of PCM and the layout mode. Kheradmand et al [17] applied the mixed phase change mortar to building facades, and tested the performance and energy conservation by a combined numerical and experimental method. Results showed that joining the phase change mortar would be helpful in reducing indoor load and maintaining the stability of the indoor temperature. Chaiyat et al [18-19] studied the concrete wall with phase change micro capsule in different areas. It was concluded that there was more load reduction in summer than that in winter, and different energy savings are demonstrated in different areas. Kong et al [20] investigated the influence of two different installation forms of shape-stabilized PCM on the indoor thermal comfort. One is the panels installed on the outside surface of walls and roofs (PCMOW) with acid capric contained, the other is the panels installed on the inside surface of walls and roofs (PCMIW) with capric acid (95 wt%) and1-dodecanol (5 wt%) contained. Their experimental and numerical results showed that the PCMIW system has a better control effect than that of the PCMOW system. Zhou et al [21] used the enthalpy model to calculate a solar room with the shape-stabilized PCM plates and then analyzed the effect of melting temperature of PCM, heat transfer coefficient, the position and thickness of PCM plates etc. on indoor temperature. They found that the PCM plate can be fully stored in the daytime and released at night to improve the indoor comfort.

Unlike common LHTESs, there are unique application environment and control target for the coupled cooling method. The coupled cooling method consists of two processes: the pre-cooling process and the coupled cooling process. And the coupled cooling process includes the heat transfer among PCM units, envelop, air and heat sources in a closed space. Therefore, to improve the operation efficiency and reduce energy consumption, the sensitivity analysis and optimization of the coupled cooling system, new tasks, should be done.

To solve the cooling problem in high-temperature, passive, impact and other harsh environments, based on the new coupled cooling method of LHTES combined with pre-cooling envelop and the numerical simulation model which considering the heat source, Surrounding Rock (SR), PCM and air heat transfer, the thermal performance of the coupled cooling method is analyzed and an evaluation parameter of heat tolerance is proposed to evaluate the temperature control effect using a mine refuge chamber as a case study. A parametric study is undertaken into exploring the impact of other factors, such as pre-cooling temperature of SR, melting temperature of PCM, aspect ratio and amounts of PCM unit, on indoor temperature in a systematic manner. Optimization of the coupled cooling system is also conducted.

2. Model and parameter settings

2.1 Mathematical model

The coupled cooling process includes the heat transfer among phase change units, SR, air and heat sources in a closed space. In the current work, the phase change units hang on the wall with the form of plates and the back ventilation is adopted to enhance the convective heat transfer. For the purpose of briefness, the following major assumptions are employed [22]: i) The ratio of the length to the width is more than 2 and the chamber is assumed to be a cylinder. ii) The heat source is constant and the effect of radiation is negligible. iii) The material of the surrounding rock is homogeneous and isotropic and neglecting the heat transfer caused by the moisture transfer through the envelope. iv) Ignore the influence of temperature fluctuation from ground surface because the embedded depth is 400~600 m. Other simplifications are described in the rest of the paper.

2.1.1. Heat transfer model of SR

The equation for calculating the changes in the temperature of SR in vector form is:

$$\frac{\partial t}{\partial \tau} = a \frac{\partial^2 t}{\partial r^2} + \frac{1}{r} \cdot \frac{\partial t}{\partial r} \tag{1a}$$

The boundary conditions are

$$\begin{cases} -\lambda_w \dfrac{\partial t(r_i, \tau)}{\partial r} = h_w \left[t_f - t(r_i, \tau) \right] \\ t(r_o, \tau) = t_0 \end{cases} \tag{1b}$$

with initial condition is

$$t(r,0) = t_0 \tag{1c}$$

where, t_0 is the initial temperature, τ is the time, a is the thermal diffusivity, r is the radius of the SR, r_i is the inner wall radius, λ_w is the thermal conductivity, t_f is the air temperature, r_o is the outer surface radius. h_w is the natural convective heat transfer coefficient between the air and inner wall, which can be calculated by the formula (2) and (3) [23]:

$$Nu = \frac{hl}{\lambda_a} \tag{2}$$

$$Nu = 0.59(Gr\,\mathrm{Pr})^{1/4} \tag{3}$$

where, Nu is the Nusselt number, l is the feature size, λ_a is the thermal conductivity of air. $Gr=g\alpha_V \Delta t l^3/v^2$ is the Grashof number, where g is the acceleration of gravity, α_V is the air volume expansion coefficient, Δt is the temperature difference, v is the dynamic viscosity, Pr is the Planck number.

2.1.2. Heat transfer model of PCM plate

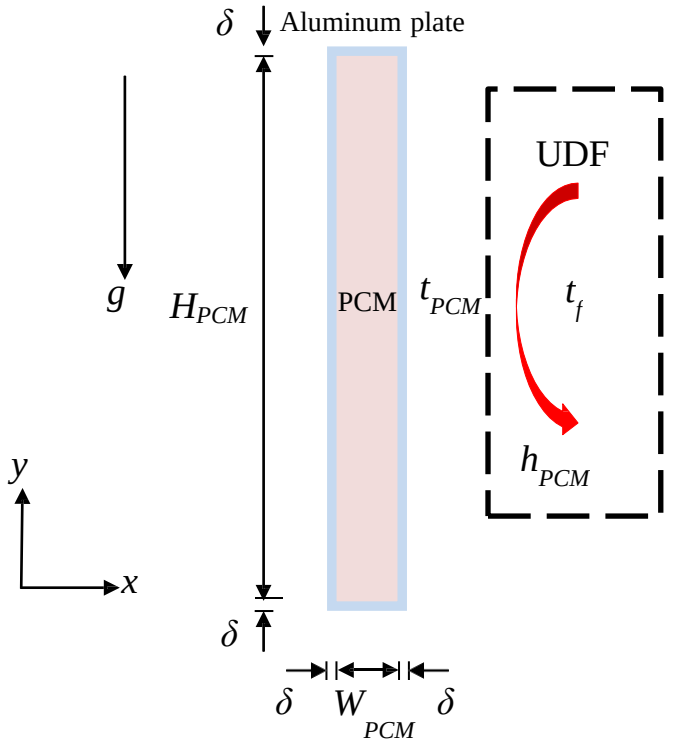

Fig. 2. Computational domain and boundary conditions at the vertical mid-plate of PCM plate.

PCMs are encapsulated by aluminum plate and the thickness of the plate is 1.5 mm. The geometry of the PCM plate is designed as follows (not including the aluminum plate): the length L_{PCM} is 600 mm, the height H_{PCM} is 500 mm, and the thickness W_{PCM} is 60 mm. As shown in Fig.2, the vertical mid-plane of the PCM plate is selected as the computational domain.

Since the PCMs are encapsulated by aluminum plate, the heat transfer of the outer aluminum surface of the PCM plate is convection, and the interface between the aluminum surface and the PCM is the coupled interface. There exists heat conduction, convection and melting processes in the PCM plate, so the enthalpy-porosity model was used to solve the two dimensional heat transfer equations. The equations of enthalpy-porosity model can be seen in Yuan et al [14].

2.1.3. Model of indoor air

The energy conservation equation is used to calculate the temperature of the air:

$$C_a \rho_a V_a \frac{\partial t_f}{\partial \tau} = q + q_w + q_{PCM} \quad (4)$$

where, C_a is the specific heat of air; q is the indoor heat flux; q_w is the convective heat flux between air and SR; q_{PCM} is the convective heat flux between air and PCM plate. q, q_w, q_{PCM} are calculated by the following formula:

$$q = N_p q_p \quad (5)$$

$$q_w = h_w A_{i,w} \left(t_w - t_f \right) \quad (6)$$

$$q_{PCM} = N_{PCM} h_{PCM} A_{PCM} \left(t_{PCM} - t_f \right) \quad (7)$$

where, N_p is the number of people in refuge chamber; q_p is per capita heat generation rate (including equipment); $A_{i,w}$ is area of the inner wall; N_{PCM} is the number of PCM plates; A_{PCM} is the area of the outer surface of one PCM plate.

2.2. Numerical solution method

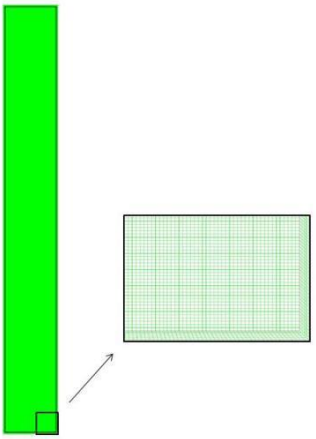

Fig. 3. Computational Grid of PCM plate.

In the current study, the heat conduction, convection and melting processes are coupled in the PCM plate, so the PCM plate model is set as the main model. The air temperature and convection heat transfer coefficient, calculated by User Define Function (UDF), are in the form of boundary conditions in the main model. The calculation model of PCM plate is 2D. The calculation software is ANSYS Fluent14.0. The calculation is based on the melting and solidification model. The influence of natural convection is considered in the PCM unit, and the density calculation is based

on the Boussinesq assumption. The heat transfer of outer aluminum surface of the PCM plate is convection, and the convection heat transfer temperature and coefficient are t_f and h_{PCM}, respectively. The interface between the aluminum surface and the PCM is the coupled interface. The time step is 1s, and the total number of steps is 345600. Fig.3 shows the 2D computational grid of PCM plate and the number of grids is 100,000.

2.3. Model validation

To verify the correctness of the numerical model, the calculated result is compared with the experimental data of Wu et al [24]. The experiment was carried out in a rectangle ferruginous box with a size of 1 m×0.9 m×1.2 m during 96 h. The indoor heat source is 170W. The initial temperature was 15℃, and 3 thermocouples were built-in to detect the temperature distribution. The melting temperature of PCM is 28℃. More PCM properties can be seen in Wu et al [24].

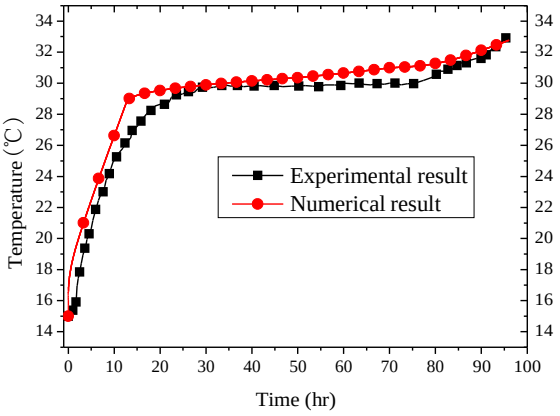

Fig. 4. Comparison of the experimental and numerical melt fractions.

Fig. 4 shows the comparison of the temperature variation between the experimental data and numerical result and close agreement is achieved. It can be seen clearly that there is a mutation when the temperature reaches 29℃ for the simulation result and that is a slow transition for the experimental result. This is because the real PCM melts in a temperature range, not at a temperature point.

2.4. Parameter settings

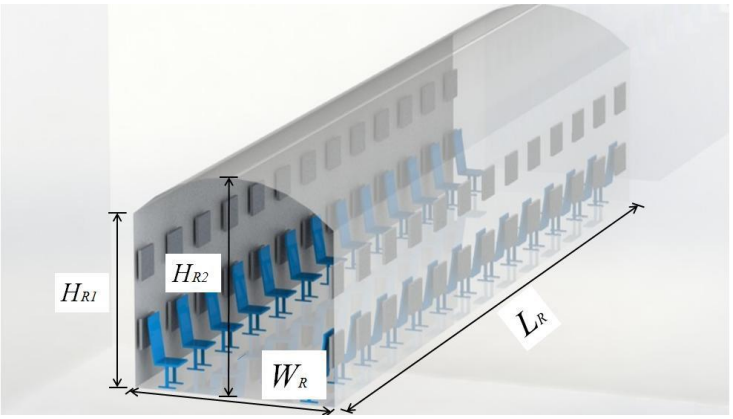

Fig. 5. Schematic diagram of 3D model of mine refuge chamber with PCM plate.

Refuge chamber is an emergency rescue system. According to the Chinese policy, the temperature inside the chamber can not exceed 35℃ within 96 h. Take the refuge chamber with 48 people as an example (shown in Fig. 5), the inner wall of the refuge chamber hangs PCM plates. Parameters of mine refuge chamber are listed in Table 2.

Table 2. Parameters of mine refuge chamber.

Symble	Description	Value	Calculation method
L_R	Length of refuge chamber	17 m	
W_R	Width of refuge chamber	4 m	
H_{R1}	Height of side wall	2.8 m	
H_{R2}	Height of vault	3.5 m	
r_i	Equivalent radius of inner wall	2 m	$r_i=(S/\pi)^{1/2}$
ρ	Density of surrounding rock	2400 kg/m^3	
c_P	Specific heat of surrounding rock	902 J/(kg·K)	
λ	Thermal conductivity of surrounding rock	2 W/(m·K)	
t_0	Initial temperature	30℃	
t_c	Control temperature	35℃	
t_{pc}	Pre-cooling temperature	25℃	
N_P	Stipulated number of personnel	48	
q_p	Heat generation of each person	116W	

PCM is RT 26 [25], and more relevant materials' parameters are summarized in Table 3. For a preliminary design of the number of PCM plates, there is a need to calculate the dynamic heat flux of SR according to the heat transfer model. Afterwards, it is calculated that the average indoor load is 1528 W. Combined data in Table 2 and PCM plate's parameter, the estimated number of PCM plates is 175. Considering the factor 1.1, the number of PCM plates is 190 as an initial calculated value.

253 Table 3. Properties of paraffin and aluminum.

Materials	Density/ kg/m^3	Thermal conductivity/ W/m·K	Specific heat/ kJ/kg·K	Melting temperature/ ℃	Latent heat/ kJ/kg	Dynamic viscosity/ kg/m·s
Paraffin	770/880 (Liquid/ Solid)	0.6	2	26-27	190	0.07
Aluminum	2719	202.4	871	-	-	-

254 # 3. Sensitivity analysis of coupled cooling system

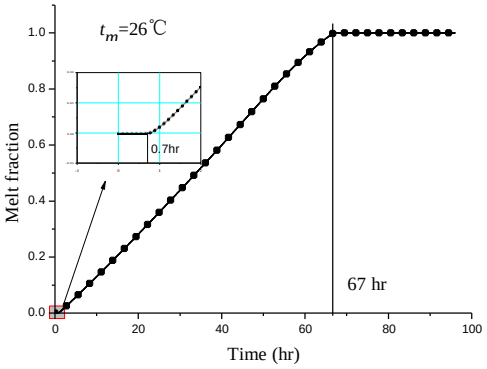

255

256 Fig. 6. Melt fraction variation within 96 hours.

257 Fig. 6 demonstrates the variation of the melt fraction within 96 hours. It is found that PCM
258 starts to melt after 0.7 hour; then the increasing rate of the melt fraction maintains unchanged and
259 followed by a minor decrease after 50 hours. Complete melts occur after 67 hours. It is believed
260 that the increasing rate of the melt fraction is mainly affected by the PCM melting process.

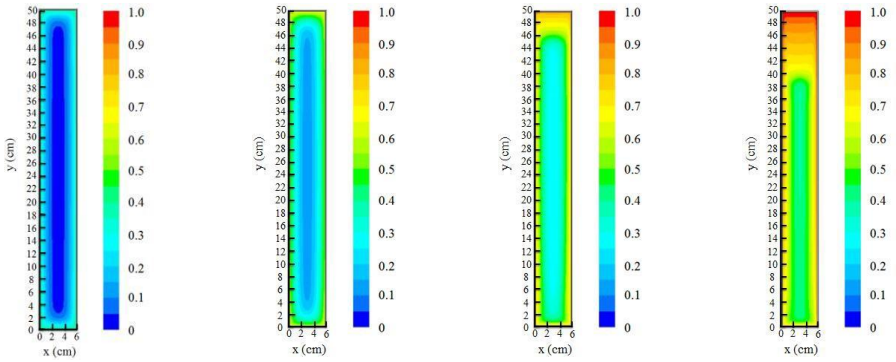

(a) Time=10hr (b) Time=20hr (c) Time=30hr (d) Time=40hr

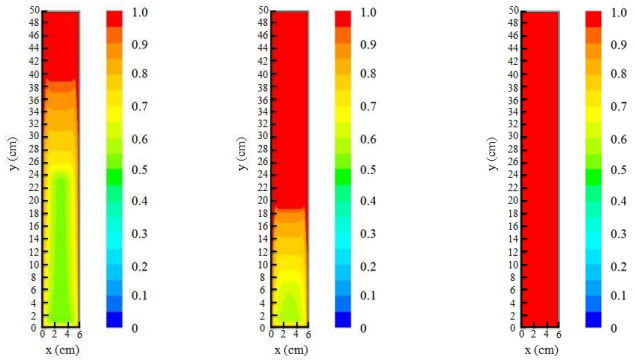

(e) Time=50hr (f) Time=60hr (g) Time=70hr

Fig. 7. Instantaneous temperature distribution at the vertical mid-plane of the PCM plate.

Fig.7 demonstrates the contour temperature distribution at the vertical mid-plane of the PCM plate at different time, i.e. 10, 20, 30, 40, 50, 60 and 70 hr. Within the first 30 hours, as shown in Figs. 7(a), 7(b), 7(c)), the isotherms almost parallel to the surface of the aluminum plates, which shows the heat transfer mode is heat conduction. Later on, as presented in Fig. 7(d), the upper of the PCM plate becomes more lateral isotherms, which shows the heat mode changes to heat convection. Afterwards, as illustrated in Figs. 7(e) and 7(f), the liquid PCM absorbs the heat and the temperature rises. With the assistance of natural convection, the liquid PCM rises along the aluminum plate. In this case, most isotherms become lateral, which means that natural convection plays the dominant role. When the time reaches 70 hour, as presented in Fig 7(g), the PCM completely melts.

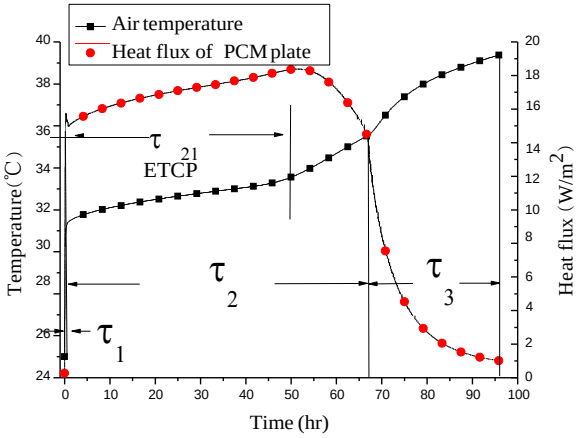

Fig. 8. Changes of air temperature and heat flux of PCM plate within 96 hours.

Fig. 8 demonstrates the variation of the air temperature and heat flux of PCM plate within 96 hours. It can be clearly noted that there exist three stages with the increase of the air temperature. At the initial temperature increase stage τ_1, within the first 0.7 hour the air temperature increases remarkable to be up to 31.4℃. At the second stage, which is the temperature control stage τ_2 from 0.7 to 67 hour, the temperature increases monotonously from 31.4℃ to 35.6℃ which represents a 4.2℃ increase. And the changes in temperature occur slowly from 0.6 hour to 50 hour. Within this Effective Temperature Control Period (ETCP) τ_{21}, the solid and liquid PCM coexist, making a stable thermal environment. Within the third stage, which is called rapid temperature increase stage τ_3, from 67 hour to 96 hour, the air temperature significantly rises by 3.8℃, finally reaching 39.4℃. The final temperature is more than 35℃ because this calculation is based on the estimated value (or initial value), which has not been optimized. The reason why the air temperature appears 3 stages is that: in the stage τ_1, the PCM plate has not yet begun to melt, and most of the heat is absorbed by air; in the stage τ_2, the air temperature is beyond the melting temperature and the PCM begins to melt and absorb heat, which makes the increasing rate of the air temperature slow down gradually; in the stage τ_3, PCM has almost been melted into liquid, and the ability to absorb heat has dropped dramatically, which leads to a significant rise of air temperature.

Meanwhile, Fig. 8 describes the surface heat flux of PCM plate. It is also noted that the heat flux of the PCM plate has three stages, which explains that the air temperature increase phases is mainly affected by the heat flux of the PCM plate. Especially from 0.7 hour to 50 hour, the heat flux of the PCM plate rises slowly by 3.4 W/m^2. In this case, the PCM uses the latent heat to make

299 the increasing rate of the air temperature slow down gradually. From 50 hour to 67 hour, the heat
300 flux of the PCM plate slowly decreases by 4.3 W/m^2. The reason could be that the melt fraction is
301 already over 80%, and the heat storage ability decreases greatly with the reduction of the
302 remaining PCM volume, which can be seen in Fig. 7. After 67 hours till the end, the PCM
303 completely melts, and the PCM can only depend on sensible heat with the speed of 1 W/m^2.
304 Within this time period, the air temperature rises greatly.

305 To evaluate the temperature control effect of the PCM plate, an evaluation parameter of heat
306 tolerance time γ is proposed, which combines the calculated result of the air temperature and the
307 formula $\tau_e=4.1\times10^8/t^{3.61}$, proposed by Cranee [26], where τ_e stands for extreme endurance time. γ is
308 defined as the ratio of actual time, during which the temperature exceeded t_c, to τ_e. Since the
309 ambient temperature does not vary greatly, the average time temperature is adopted instead of time
310 variation temperature for the sake of formula's simplicity. Besides, as previously mentioned,
311 Chinese government states that the indoor temperature in the refuge chamber must not exceed
312 35℃, which means t_c=35℃. Therefore, the formula is defined as follows:

313
$$\gamma=\frac{\tau_{>35}}{\tau_e}=\frac{\tau_{>35}\cdot\bar{t}_{>35}^{\,3.61}}{4.1\times10^8} \tag{8}$$

314 where, $\tau_{>35}$ refers to the time that temperature is over 35℃ and $\bar{t}_{>35}$ is the average temperature
315 that the indoor temperature is over 35℃.

316 It can be seen from the definition that the smaller the γ, the better the temperature control.
317 When γ is zero, casualty will not be caused under such temperature; when γ is close to 1, human
318 body's extreme endurance appears and this will endanger human's life; when γ is over 1, human
319 body's extreme endurance exceeds.

320 In order to maximize the usage of the thermal storage ability of PCM, and match the heat
321 flux of the thermal storage and indoor load, there is a need to analyze the impact factors, such as
322 pre-cooling temperature, melting temperature of PCM, size and amounts of PCM plates. In the
323 current work, an evaluation parameter of heat tolerance time γ is used. For each analysis, only one
324 factor is changed and keeps the other factors unchanged.

3.1. Effect of pre-cooling temperature

It is believed that the pre-cooling temperature t_{pc} can affect the PCM quantity. Thus, it is necessary to observe the changes of the indoor estimated load at different t_{pc}. Here, the indoor estimated load refers to the cold that PCM should bear. The finite volume method is used to calculate the rising temperature of the SR at different t_{pc}, and then the indoor estimated load is calculated. As for the indoor natural convection simulation, the average indoor wind speed is set to be 0.1 m/s, the stable indoor temperature is 35℃, and six different t_{pc}, i.e. 24℃, 25℃, 26℃, 27℃, 28℃ and 29℃ are employed in the current study.

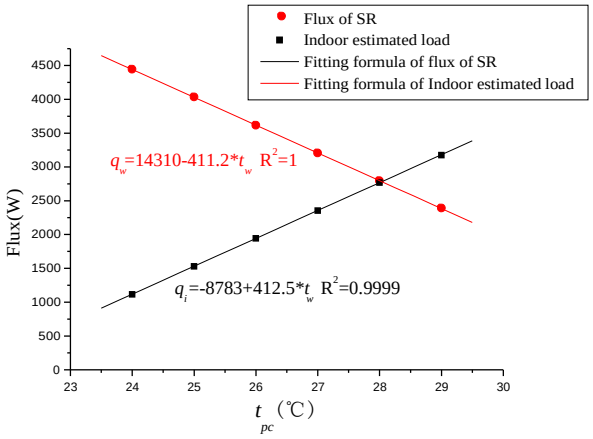

Fig. 9. Average heat flux of SR and indoor estimated load versus t_{pc} and their fitting curves.

Fig.9 presents the variation of the average heat flux of SR q_w and average indoor estimated load q_i as a function of t_{pc}. It can be seen, as expected, that both the average flux of SR q_w and average indoor estimated load q_i are a linear function of the t_{pc}. If the t_{pc} increases from 24℃ to 29℃, the average indoor estimated load will increase from 1114 W to 3175 W, which equals to a 185% increase. And the average flux of SR decreases from 4443 W to 2389 W, then it equals to a 46% decrease. Their fitting formulas are showed as follows:

$$q_w = 14310 - 411.2 \times t_w \qquad \left(R^2 = 1\right) \tag{9}$$

$$q_i = -8783 + 412.5 \times t_w \qquad \left(R^2 = 0.9999\right) \tag{10}$$

Here, q_w decreases as the t_{pc} increases. When q_w=0, SR has no cold release, that it, the initial temperature of SR is 35℃. According to Eq. (9), it can be calculated that t_w=34.8℃, which is close to 35℃, meaning that the fitting formula is reliable. The indoor estimated load q_i increases

gradually as the t_{pc} increases. When q_i=0, indoor load is completely absorbed by the SR. Based on Eq. (10), it can be calculated that t_w=21.3℃. Namely, when the t_{pc} lowers than 21.3℃, the indoor hear load is zero, in this case the cooling system is not necessary.

3.2. Effect of melting temperature

It is recognized that the melting temperature is a key parameter to affect the thermal property of the PCM plate. In order to investigate the effect of the size , in the current work, the other parameters are kept the same: t_{pc}=25℃, N_{PCM}=190, the size of PCM plate is 600 mm in length, 60 mm in width and 500 mm in height and the PCM's density, latent heat, thermal conductivity and specific heat maintain constant. The simulation is carried out with the melting temperature increases from 26℃ to 31℃.

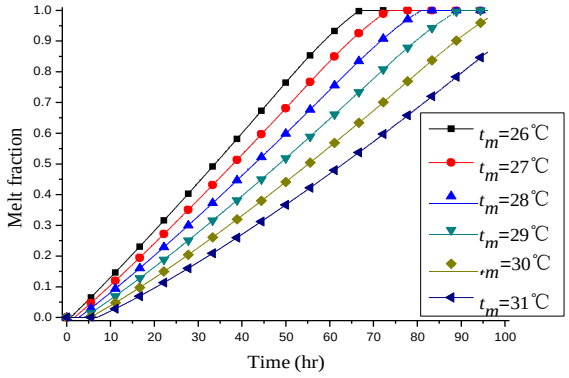

Fig. 10. Melt fraction curves at different melting temperatures.

Fig.10 depicts the evolution of the melt fraction of PCM with time at six different melting temperatures. In Fig. 10, it can be obviously observed that at the fixed time, the melt fraction gradient is low as the melting temperature increases, It can be seen from Fig. 10 that when the melting temperature varies from 26℃ to 29℃, all the PCM completely melts within 96 hours, and the melting time is 67.0 h、73.5 h、80.9 h and 89.5 h respectively. When the melting temperature reaches 30℃ and 31℃, the results in Fig. 10 clearly show that the PCM does not completely melt, and the computed final melt fraction is approximately 0.974 and 0.864 respectively. The reason could be that when the melting temperature increases, the air temperature will increase at the same time, which will lead to the heat transfer of air towards SR increase. As the thermal storage of PCM decreases, the melting rate slows down.

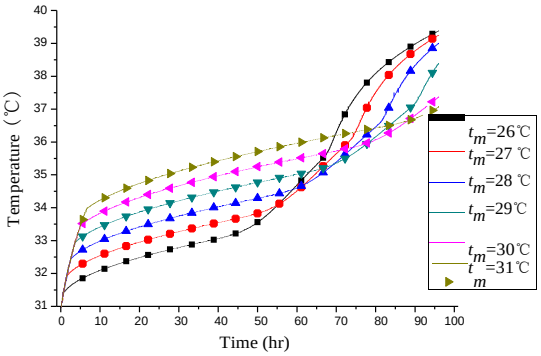

Fig. 11. Hourly indoor temperatures for varies melting temperatures.

Fig.11 demonstrates the variations of indoor temperature as a function of time at six different melting temperatures, i.e., 26℃, 27℃, 28℃, 29℃, 30℃ and 31℃. Sensitivity analysis in Fig.11 shows that, as the melting temperature increases, the temperature of ETCP will rise and the duration will extend. It should be noted that when the melting temperature increases from 26℃ to 31℃, the average temperature of ETCP improves about 0.47℃, 0.46℃, 0.45℃, 0.45℃ and 0.43℃ respectively, and the duration lengthens about 6.5 h, 7.9 h, 7.1 h, 10.9 h and 13.1 h respectively. When the melting temperature reaches 30℃ and 31℃, the air temperature rising stages only involve initial temperature increase stage τ_1 and temperature control stage τ_2. The reason could be that, according to the Newton cooling formula, when the temperature difference of the air and the PCM is $\Delta t=t_f-t_m$, the PCM will absorb heat $q_{PCM}=h_{PCM}A_{PCM}\Delta t$. When the t_m increases, the air temperature t_f will increase accordingly.

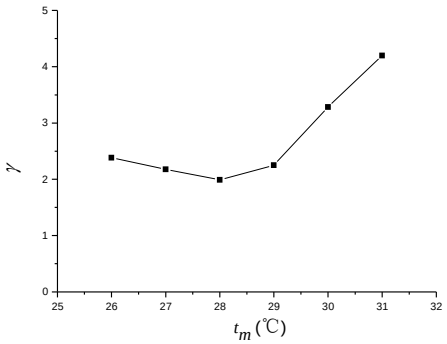

Fig. 12. γ varies with melting temperature.

γ can be used to evaluate the effect of temperature control. Fig.12 depicts the evolution of the evaluation parameter γ with melting temperature. It should be noticed that the γ value at every t_m is greater than 1 because this calculation is based on the estimated value (or initial value), which has

not been optimized. As stated previously, six different melting temperatures, i.e. 26℃, 27℃, 28℃, 29℃, 30℃ and 31℃ are explored in the current study. It can be seen clearly from Fig. 9 that the γ decreases from 26℃ to 28℃. Starting from 28℃ till the end, there is a quick increase of γ. As is always the case, the melting temperature cannot be too high or too low. In the current study, the γ reaches the lowest at t_m=28. Therefore, in the following sensitivity analyses, t_m=28 is chosen as the calculated value.

3.3. Effect of size of PCM plate

Even with the same volume, different unit sizes show different influences on the heat transfer and melting processes. In order to investigate the effect of the size , in the current work, the other parameters are kept the same: t_{pc}=25℃, t_m=28℃, N_{PCM}=190, the length of PCM is 600 mm, and the PCM's density, latent heat, thermal conductivity and specific heat maintain constant. Under the operating conditions studied, four aspect ratios, i.e. W50H600, W60H500, W70H429, and W80H375 are investigated, respectively.

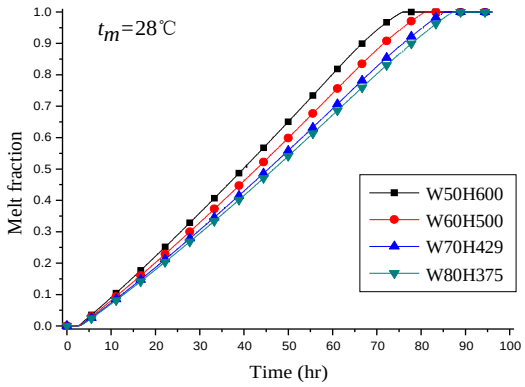

Fig. 13. Melt fractions at different aspect ratios.

Fig.13 demonstrates the variation of melt fraction with time at four different aspect ratios at t_m=28℃. It is noted that when the aspect ratio of PCM plate changes from 50/600 to 80/375, the melting time is 75.9 h, 80.9 h, 85.3 h and 87.2 h respectively. According to the curves presented in Fig.13, it could be concluded that the melting time increases with the increase of the aspect ratio during the early stage. However, further increasing the aspect ratio (>70/429) would result in the decrease of the melting time rate. The reason could be that the change of the aspect ratio will lead to the change of the area of PCM plate. The larger the aspect ratio is, the smaller the surface area

is. According to the Newton cooling formula, the decrease of the area will reduce the heat absorption of the PCM. Then the melting rate of PCM will also slow down. As the variation of surface area is not large, it can be seen from Fig.13 that the change of melting rate is also not obvious.

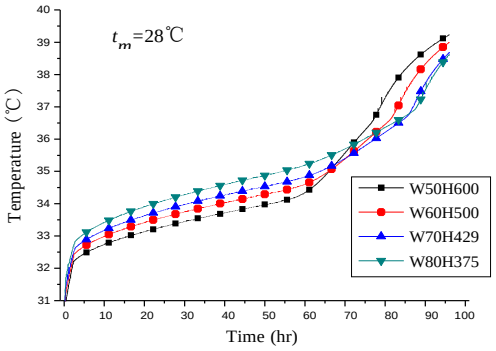

Fig. 14. Hourly indoor temperature for varies aspect ratios.

Fig.14 illustrates the variation of indoor temperature with time at four different aspect ratios and fixed melting temperature of 28℃. Obviously, the indoor temperature increases monotonously during the entire process. It is found that the increase of the aspect ratio will improve the temperature of ETCP as well as lengthen the time. When the aspect ratio changes from 50/600 to 80/375, the temperature of ETCP increases by 0.38℃, 0.23℃ and 0.32℃. For the case of the aspect ratio is more than 70/429, the duration of ETCP does not lengthen. The reason is that the bigger the aspect ratio, the smaller the surface area A_{PCM}. According to the Newton cooling formula, when the A_{PCM} decreases, the temperature difference Δt will increase accordingly. And the t_m is a constant value, so the air temperature t_f will increase.

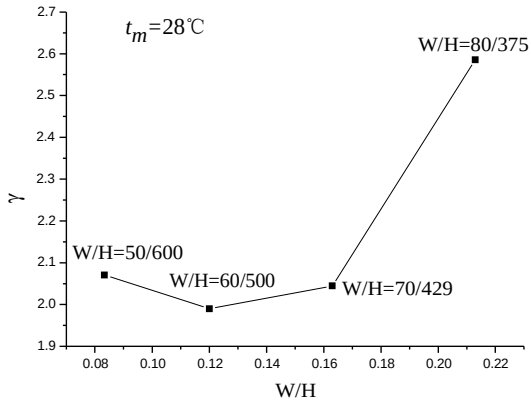

Fig. 15. γ changes with different aspect ratios.

Fig.15 demonstrates the variation of evaluation parameter γ for aspect ratios of 0.083, 0.12, 0.163 and 0.213 at fixed melting temperature of 28℃. It should be noted that the γ value at every W/H ratio is greater than 1 because this calculation is based on the estimated value (or initial value), which has not been optimized. The general trend for γ variation is similar to that observed in Fig. 12. It should be also noted that there exists an optimal value of PCM size. From Fig.15, it is demonstrated that when the aspect ratio is too low, the duration of ETCP is short, and the temperature increases quickly in τ_3; whereas the aspect ratio is too high, the temperature of ETCP is too high, and the duration does not lengthen.

3.4. Effect of number of PCM plates

In order to reduce the consumption of PCM and the cost as well as the occupied volume, to seek a minimum number of PCM plates becomes a very important issue. In this study, sensitivity analysis is conducted for seven different numbers of PCM plates: 190, 210, 228, 245, 262, 280, 298, and other parameters are kept the same: t_{pc}=25℃, t_m=28℃, the size of PCM unit is L600W60H500, PCM's density, latent heat, thermal conductivity and specific heat maintain constant.

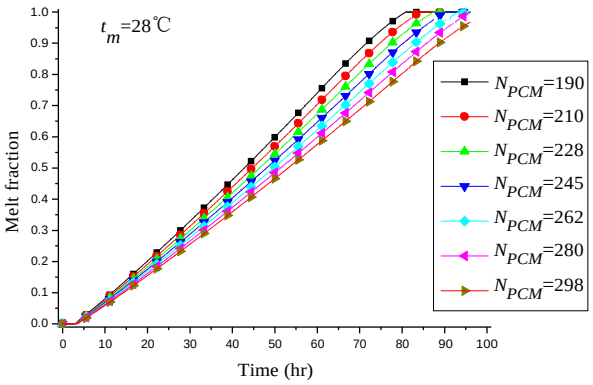

Fig. 16. Melt faction at different numbers of PCM plates.

Fig.16 demonstrates the melt fraction plotted with respect to the time at seven different numbers of PCM plates and fixed melting temperature of 28℃. Under the operating conditions studied, obviously, the larger the number of PCM plates, the longer the melting time. According to the curves presented in Fig.16, it is shown that when N_{PCM} increases from 190 to 298, the complete melting time is 80.9 h, 84.3 h, 87.4 h, 90.3 h, 93.3 h and 96 h respectively. As also shown in this

figure, when N_{PCM} is 298, PCM does not completely melt.

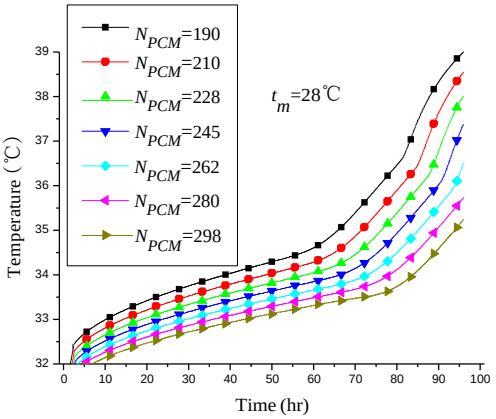

Fig. 17. Hourly indoor temperatures for different numbers of PCM plates.

Fig.17 illustrates the variation of indoor air temperature at seven different numbers of PCM plates, i.e. 190, 210, 228, 245, 262, 280 and 298, under the constant melting temperature (28℃). It is proved that the increase of N_{PCM} will reduce the temperature of ETCP. When N_{PCM} increases from 190 to 298, the temperature of ETCP will decrease by 0.24℃, 0.19℃, 0.17℃, 0.17℃, 0.15℃ and 0.15℃ respectively; while the duration lengthens 2.8 h, 2.6 h, 2.4 h, 2.5 h, 2.5 h and 2.5 h respectively. The reason could be that the A_{PCM}, total heat transfer area of PCM, increases with the increase of the N_{PCM}. According to the Newton cooling formula, when the A_{PCM} increases, the temperature difference Δt will decrease accordingly. And the t_m is a constant value, so the air temperature t_f will decrease, which results in a lower air temperature. Furthermore, the increase of the N_{PCM} will also improve the total latent heat of PCM, so the duration of ETCP will lengthen accordingly.

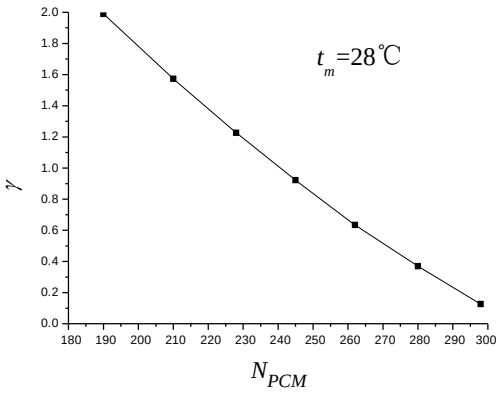

Fig. 18. γ changes with different N_{PCM}.

Fig.18 illustrates the effect of number of PCM plates on the evaluation parameter γ at fixed melting temperature of 28℃. Under the operating conditions studied, seven different numbers of PCM plates, i.e. N_{PCM} =190, 210, 228, 245, 262, 280 and 298, are investigated. As shown in Fig.18, this plot suggests that γ is nearly inversely proportional to the number of PCM plates. The bigger the number of PCM plates, the lower the γ value. When N_{PCM} changes from 190 to 298, the γ value is 1.99, 1.57, 1.23, 0.92, 0.63, 0.37 and 0.13 respectively. This result may be attributed to the increase of the number of PCM can not only reduce the temperature of ETCP, but also increases the duration. The number of PCM plates has positive effect on temperature control, but the higher the number, the higher the cost. To save energy consumption and cost, the next part of the paper is to achieve the temperature control with the minimum number of PCM plates and other optimal parameters.

4. Optimization of coupled cooling system

There exist three stages with the increase of the air temperature. First, the initial temperature increase stage τ_1 that the indoor load is mainly absorbed by air. Then the temperature control stage τ_2 that PCM begins to melt and absorb heat, assisted by thermal storage of SR. Finally, the rapid temperature increase stage τ_3 that PCM completely melts, only rely on the thermal storage of SR. Besides, there is an obvious stage τ_{21}, which is called ETCP, during which the air temperature slowly increases. Since the air temperature increases quickly after the ETCP, the increase of the air temperature is hoped to stay in τ_1 and τ_{21} and the curve of the air temperature is called the target temperature curve. Fig.19 shows the comparison between the original temperature curve and target temperature curve.

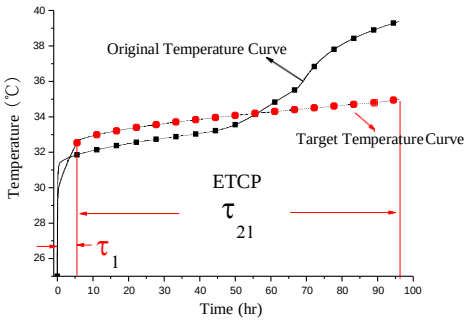

Fig. 19. Target air temperature rise curve.

It can be seen from the original temperature curve in Fig.19 that the temperature of ETCP and the lengthening duration should be balanced in order to make it close to the target temperature curve. Based on previous sensitivity analysis, t_{pc} presents linear influence on the indoor load; the rise of melting temperature and the increase of aspect ratio will cause the temperature to rise and the duration lengthens in ETCP; the increase of N_{PCM} can lower temperature and lengthen the duration of ETCP at the same time, but the larger the N_{PCM}, the higher the cost. Therefore, the optimal values of melting temperature and aspect ratio should be selected and a minimum number of PCM plates are essential.

Combined optimization with double factors is adopted for reducing computation load. And the sensitivity analysis shows that the size of the PCM plate has the least influence on the temperature control. Therefore, first, the combination optimization with the melting temperature and the size of PCM plate is conducted to find the optimal size of PCM plate. Then with the optimal size of PCM plate, the combination optimization with the melting temperature and the number of PCM plates is conducted to find the optimal melting temperature and minimum number of PCM plates. Finally, the optimal design is also conducted for different t_{pc} with the optimal size of PCM plate.

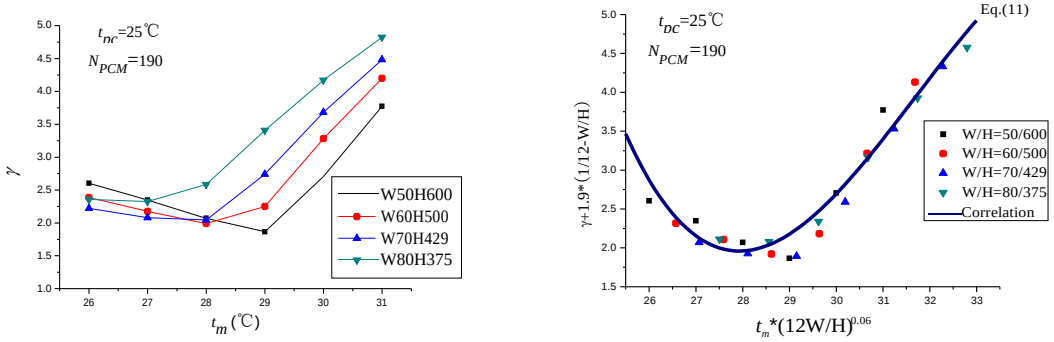

(a) (b)

Fig. 20. Generalized results for the γ at various melting temperature and different aspect ratio: (a) γ versus t_m;(b) γ versus t_m* $(12W/H)^{0.06}$.

Fig.20(a) shows the variation of γ with melting temperature ranges from 26℃ to 31℃ at fixed pre-cooling temperature (t_{pc}) of 25℃ and number of PCM plates (N_{PCM}) of 190. For comparison purpose, four aspect ratio conditions are used in this study, i.e. W/H=0.083, 0.12, 0.163 and 0.213. When the melting temperature is lower than 28℃, the influence of variation of

aspect ratio on γ does not change monotonically. While the melting temperature is over 28℃, the greater the W/H, the smaller the γ. When the melting temperature is within 26~28℃, if γ is arranged from low to high, the W/H value is 70/429, 60/500, 50/600 and 80/375 respectively; when the melting temperature is within 29~31℃, if γ is arranged from low to high, the W/H value is 50/600, 60/500, 70/429 and 80/375 respectively. Because γ is quite small in any kind of melting temperature when W/H=60/500, the proportion of the aspect ratio should be the optimal.

In order to further explore the general principle that γ changes with the temperature under different aspect ratios, Fig.20(b) demonstrates the generalized results for the γ at various melting temperature and different aspect ratios. In order to investigate the relationship between the γ and the melting temperature, under different aspect ratios, the following correlation, using the method of curve fitting is proposed in Eq. (11).

$$\gamma + 1.9(1/12 - W/H) = a_1 x^3 + a_2 x^2 + a_3 x + a_4 \qquad R^2 = 0.956 \qquad (11)$$

where, $x = t_m*(12W/H)^{0.06}$, a_1=-0.01863, a_2=1.771, a_3=-55.33, a_4=571.7.

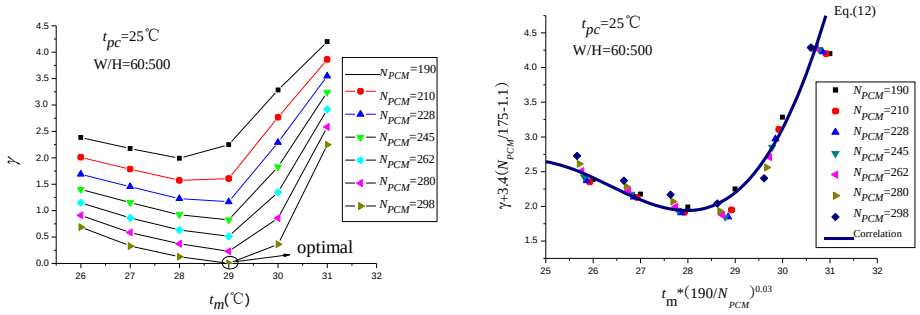

(a) (b)

Fig. 21. Generalized results for the γ at various melting temperature and different numbers of PCM plates: (a) γ versus t_m; (b) γ versus $t_m*(190/N_{PCM})^{0.03}$.

Fig.21(a) shows the distribution of γ with different melting temperature at seven different $N_{PCM,}$ i.e. 190, 210, 228, 245, 262, 280 and 298 for a fixed t_{pc}=25℃ and W/H=0.12. As expected, the result shows that N_{PCM} has a monotonic effect on γ at any melting temperature. In the current work, the optimal melting temperature is 29℃, and the minimum number of PCM plates is 298. There could be three reasons to explain why the final minimum N_{PCM} is much larger than the estimated number. Firstly, the average temperature of ETCP should be 1~2℃ lower than t_c; Secondly, no more than 80% of PCM is allowed to melt to ensure that the temperature increases

process takes place in τ_1 and ETCP. Most importantly, the indoor estimated load is actually greater for the existence of the heat storage of PCM. Therefore, a larger number of PCM plates should be selected than the estimated one.

For the purpose of briefness and engineering application, Fig.21 (b) demonstrates the generalized results for the γ at various melting temperature and different numbers of PCM plates. Under different N_{PCM}, Eq. (12) fits for all the cases that γ changes with melting temperature.

$$\gamma + 3.4(N_{PCM}/175 - 1.1) = a_1 x^3 + a_2 x^2 + a_3 x + a_4 \qquad R^2 = 0.967 \qquad (12)$$

where, $x = t_m * (190/N_{PCM})^{0.03}$, a_1=0.042, a_2=-3.297, a_3=86.540, a_4=-751.950.

Table 4. The optimal melting temperature and the minimum number of PCM plates in three different t_{pc}.

t_{pc}/℃	Melting temperature/℃	Minimum number of PCM plates
25	29	298
24	29	243
23	29	192

For the purpose of comparison, optimal design is also conducted for other two t_{pc} of 23℃ and 24℃, with the PCM plate size of W60H500L600. Table 4 lists the optimal design of PCM plate. The result clearly shows that the optimal PCM temperature needs to be kept at 29℃, the minimum number of PCM plates gradually drops as the pre-cooling temperature gradually slows down. If per 1℃ decrease in pre-cooling temperature, the final demand of PCM plates can drop 18% and 20% respectively. And as showed in Fig. 22, compared with the traditional LHTES systems (indoor thermal load is entirely borne by the PCM), the usages of PCM saved by the coupled cooling method are 58.7%, 66.3% and 73.4%, when t_{pc} are 25℃, 24℃ and 23℃.

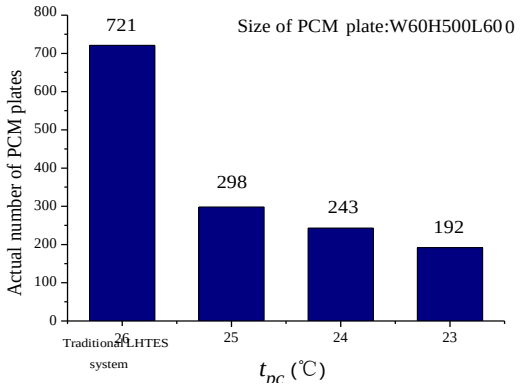

Fig. 22. Comparison of PCM usages.

5. Conclusions

This study focuses on the new free coupled cooling method of LHTES combined with PE used in mine refuge chamber. Based on the coupled cooling method and system simulation model, the thermal performance of the new coupled cooling method is investigated. Then, the effects of some impact factors, such as pre-cooling temperature, melting temperature, size and number of PCM plates are investigated, and the coupled cooling system is optimized. Several conclusions could be summarized as follows:

(1) There exist three stages with the increase of the air temperature: initial temperature increase stage τ_1, temperature control stage τ_2 and rapid temperature increase stage τ_3. The effect of temperature control would decrease significantly if PCM melts more than 80%. Therefore, it is better to make the melt fraction no more than 80% in the selection of the number of PCM plates.

(2) The melting temperature and size of PCM plates should be optimized. And for the conditions in this paper, the appropriate melting temperature is about 29℃ and the aspect ratio is 60/500.

(3) The lower the pre-cooling temperature, the smaller the indoor load, the relationship of which presents linear. In this paper, when cold temperature lowers than 21℃, there is no need of any cooling system. If per 1℃ decrease in pre-cooling temperature, the actual demand of PCM plates drops about 19%.

(4) For convenient application, the generalized results for the evaluation parameter of heat tolerance time γ at various melting temperature under different aspect ratios and N_{PCM} are given, respectively.

(5) The PCM plates absorb the pre-cooling cold and discharge it during the working time, which does improve the indoor thermal comfort degree. The use of PCM saved by the coupled cooling method is more than 50% compared to the traditional LHTES systems.

The result demonstrates that the new coupled cooling method can effectively control the indoor temperature and reduce the use of PCM under the condition of high-temperature and no-power. However, the cooling capacity of PCM is not matched with hourly indoor load. Therefore, it is suggested that the whole heat transfer process should be fully taken into consideration when the coupled cooling method is used. And it is better to lower the pre-cooling

582 temperature. Besides, there is a need to optimize PCM unit's parameter. The results of this paper
583 are expected to be useful for the design and application of the coupled cooling method of LHTES
584 combined with PE and other similar LHTESs.

585 Acknowledgements

586 Authors would like to thank the project of the National Natural Science Foundation of China
587 entitled "A study of the characteristics of the surrounding rock cold storage-phase-change heat
588 storage coupled cooling system for mine refuge chambers" (NO. 51378426), the Youth Science
589 and Technology Innovation Team of Sichuan Province of Building Environment and Energy
590 Efficiency (No. 2015TD0015) and the National Natural Science Foundation of China and the
591 Royal Society International Exchange Program entitled "Research of heat transfer characteristics
592 of refuge chamber based on coupling multi factors" (No. 5141101198)for the financial support for
593 this study.

594 References

595 [1] Zhang Z, Yuan Y, Wang K. Effects of number and layout of air purification devices in mine
596 refuge chambers. Process Saf Environ Prot. 2016. DOI: 10.1016/j.psep.2016.11.023.
597 [2] Zhang Z, Yuan Y, Wang K, Gao X, Cao X. Experimental investigation on influencing factors of
598 air curtain systems barrier efficiency for mine refuge chamber. Process Saf Environ Prot.
599 2016;102:534-546.
600 [3] Piao M, Mao J, Wang T. Status quo and prospect of the development for underground coal
601 mine refuge chamber. J Coal Sci Eng. 2013;19(1):38-45.
602 [4] Kielblock AJ, Van RJP, Van DLA. Functional performance of formal gold mine and colliery
603 refuge bays with special reference to air supply failure. J Mine Ventilation Soc S Afr.
604 1988;41(5):58-70.
605 [5] Yuan Y, Gao X, Wu H, Zhang Z, Cao X, et al. Coupled Cooling Method and Application of
606 Latent Heat Thermal Energy Storage Combined with Pre-cooling of Envelope: Method and Model

607 Development. Energy. 2017;119:817-833.
608 [6] Barzin R, Chen JJJ, Young BR, Farid MM. Peak load shifting with energy storage and
609 price-based control system. Energy. 2015;92:505-514.
610 [7] Gowreesunker BL, Tassou SA. Effectiveness of CFD simulation for the performance
611 prediction of phase change building boards in the thermal environment control of indoor spaces.
612 Build Environ. 2013;59:612-625.
613 [8] Gracia AD, Navarro L, Castell A, Cabeza LF. Numerical study on the thermal performance of
614 a ventilated facade with PCM. Energy Convers Manage. 2013;61:372-380.
615 [9] Ramakrishnan S, Wang X, Sanjayan J, Wilson J. Thermal performance of buildings integrated
616 with phase change materials to reduce heat stress risks during extreme heat wave events. Appl
617 Energy, 2016.
618 [10] Fernandes MS, Brites GJVN, Costa JJ, Gaspara AR, Costa VAF. Modeling and parametric
619 analysis of an adsorber unit for thermal energy storage. Energy. 2016; 102:83-94.
620 [11] Iten M, Liu S, Shukla A. Experimental study on the thermal performance of air-PCM unit.
621 Build Environ. 2016;105:128-139.
622 [12] Peng H, Dong H, Ling X. Thermal investigation of PCM-based high temperature thermal
623 energy storage in packed bed. Energy Convers Manage. 2014; 81:420-427.
624 [13] Jin X, Zhang S, Xu X, Zhang X. Effects of PCM state on its phase change performance and
625 the thermal performance of building walls. Build Environ. 2014; 81:334-339.
626 [14] Yuan Y, Cao X, Xiang B, Du Y. Effect of installation angle of fins on melting characteristics
627 of annular unit for latent heat thermal energy storage. Sol Energy. 2016;136:365-378.
628 [15] Borderon J, Virgone J, Cantin R. Modeling and simulation of a phase change material system
629 for improving summer comfort in domestic residence. Appl Energy. 2015;140:288-296.
630 [16] Solgi E, Fayaz R, Kari BM. Cooling load reduction in office buildings of hot-arid climate,
631 combining phase change materials and night purge ventilation. Renew Energy. 2016;85:725-731.
632 [17] Kheradmanda M, Azenha M, Aguiar JLBD, Krakowiak KJ. Thermal behavior of cement
633 based plastering mortar containing hybrid microencapsulated phase change materials. Energy
634 Build. 2014;84:526-536.
635 [18] Thiele AM, Jamet A, Sant G, Pilon L. Annual energy analysis of concrete containing phase
636 change materials for building envelopes. Energy Convers Manage. 2015;103:374-386.

637 [19] Chaiyat N, Kiatsiriroat T. Energy reduction of building air-conditioner with phase change
638 material in Thailand. Case Studies Therm Eng. 2014;4:175-186.
639 [20] Kong X, Lu S, Li Y, Huang J, Liu S. Numerical study on the thermal performance of building
640 wall and roof incorporating phase change material panel for passive cooling application. Energy
641 Build. 2014;81:404-415.
642 [21] Zhou G, Zhang Y, Lin K, Xiao W. Thermal analysis of a direct-gain room with
643 shape-stabilized PCM plates. Renew Energy. 2008;33:1228-1236.
644 [22] Xiao Y, Liu X, Zhang R. Calculation of transient heat transfer through the envelope of an
645 underground cavern using Z-transfer coefficient method. Energy Build. 2012;48:190-198.
646 [23] Dai G. Heat transfer. Higher Education Press, Beijing. 1999. (In Chinese.)
647 [24] Wu B, Lei B, Zhou C, Zhao Z. Experimental study of phase change material's application in
648 refuge chamber of coal mine. Procedia Engineering. 2012; 45:936-941.
649 [25] RUBITHERM. ORGANIC PCM – RT. Available from:
650 www.rubitherm.eu/en/index.php/productcategory/organische-pcm-rt/ (accessed 22.08.16)
651 [26] Huo R, Hu Y, Li Y. Introduction to building fire safety engineering. University of Science and
652 Technology of China Press, Hefei. 2009. (In Chinese.)

Table captions

Table 1. Evaluation and application of four cooling methods.

Table 2. Parameters of mine refuge chamber.

Table 3. Properties of paraffin and aluminum.

Table 4. The optimal melting temperature and the minimum number of PCM plates in three different t_{pc}.

Figure captions